INVESTIGATION OF ROTATING MODE BEHAVIOR IN BWR OUT-OF-PHASE LIMIT CYCLE OSCILLATIONS – PART 1: REDUCED ORDER MODEL*

A. Wysocki,**
Oak Ridge National Laboratory, Oak Ridge, TN, USA
wysockiaj@ornl.gov

A. Manera, T. Downar
University of Michigan, Ann Arbor, MI, USA
manera@umich.edu; downar@umich.edu

J. March-Leuba
MRU, Knoxville, TN, USA
jose.march-leuba@outlook.com

ABSTRACT

Previous neutronic/thermal-hydraulic (TH) coupled numerical simulations using full-core TRACE/PARCS and SIMULATE-3K BWR models have shown evidence of a specific "rotating mode" behavior (steady rotation of the symmetry line, i.e. constant phase shift of approximately 90 degrees between the first two azimuthal modes) in out-of-phase limit cycle oscillations, regardless of initial conditions and even if the first two azimuthal modes have different natural frequencies. This suggests a nonlinear coupling between these modes; otherwise, the phase shift between these modes would change at a constant rate during the limit cycle. The goal of the present work is to gain further insights on the rotating mode behavior using a simplified mathematical model which contains all of the important physics for this application while providing sufficient flexibility and simplicity to allow for in-depth understanding of the underlying phenomena. This was accomplished using a multi-channel, multi-modal reduced-order model, using a modification of the fixed pressure drop boundary condition to simulate channel coupling via the inlet and outlet plena, in order to destabilize the out-of-phase mode over the in-phase mode. Examination of the time-dependent solution of the nonlinear system showed a clear preference for rotating mode behavior in the four-channel model under stand-alone TH conditions and for conditions with weak neutronic feedback. When neutronic feedback was strengthened (i.e., larger reactivity feedback coefficients), the side-to-side mode (stationary symmetry line) was favored instead. Additional analyses using higher-fidelity numerical modeling, as well as a physical explanation for the rotating behavior seen in both sets of analyses, will be provided in a companion paper ("Part 2").

KEYWORDS
BWR stability, limit cycle, rotating mode, out-of-phase oscillations, reduced-order model

---

** Corresponding author

1. INTRODUCTION

Instability events in operating boiling water reactors (BWRs) have most commonly been associated with the coupled neutronic-thermal-hydraulic (TH) instability phenomenon, involving density-wave oscillations coupled with neutron kinetic feedback [1]. Typically, the core will oscillate under one of two primary classifications: in-phase (core-wide) oscillations, in which the oscillations in all fuel bundles occur with the same phase, and out-of-phase (regional) oscillations, in which one-half of the core oscillates 180° out-of-phase relative to the opposite half at any given point in time. If unmitigated, the oscillations will typically grow until reaching an asymptotic limit cycle behavior*, with a fixed amplitude and periodic behavior determined by the nonlinear dynamics of the underlying neutronic and TH equations**.

The line of symmetry dividing the two halves during out-of-phase oscillations need not be stationary, as has been observed, e.g., in the Leibstadt (KKL) September 1990 stability test [2] and detected in a natural circulation test performed in the Oskarshamn-3 BWR [3]. In the latter study, according to the authors, a clear "rotating mode" behavior was observed, at least for a time, in which the symmetry line rotated with more or less constant angular velocity, until the behavior suddenly switched into a "side-to-side" behavior characterized by a stationary symmetry line. As has been elaborated by previous authors [4] [5], the rotating case can be interpreted in terms of a superposition of the first two azimuthal modes of the static neutron flux distribution, where a 90° phase shift between the time-dependent amplitudes of these two modes is associated with a continuous rotation of the symmetry line over time (one complete rotation occurs over one oscillation period); this is what is meant by the "rotating mode" discussed above. Conversely, a 0° phase shift between the first and second azimuthal modes is associated with a stationary line of symmetry, herein referred to as the "side-to-side" oscillation mode. For intermediate phase shifts between these values, the orientation of the line of symmetry changes continuously with a non-constant angular velocity, with the superimposed behavior appearing more "side-to-side"-like or "rotating"-like depending on the proximity of the phase shift to 0° or 90°, respectively.

In the literature, it has typically been assumed that the first two azimuthal modes oscillate independently of each other during out-of-phase oscillations, with neither mode influencing the time-dependent phase of the other. In this case, the time-dependent amplitude of each azimuthal mode would oscillate at its own natural frequency (which may be different for each mode due to asymmetric fuel loading or burnup conditions), with an arbitrary and continuously changing phase shift relative to the other mode. For example, consider a BWR core in which the first azimuthal mode has a 10% shorter natural oscillation frequency than the second azimuthal mode; if at a given point in time the two modes were to oscillate in-phase, then after the first azimuthal mode completes one full oscillation period, the second mode would have a 36° phase lag relative to the first mode. Every subsequent oscillation period would add an additional 36° phase lag between the modes, until after the 10th period the two modes would once again oscillate in-phase. In this hypothetical case, the core would oscillate in a predominantly side-to-side fashion at certain times and a predominantly rotating fashion at other times, with gradual transitions between the two.

---

* Only supercritical Poincaré-Andronov-Hopf bifurcations will be considered in this study, which are characterized by a bounded limit cycle amplitude [10] [17] [18] [19]. The possible occurrence of unbounded subcritical bifurcations is beyond the scope of the present study.

** It has been suggested by some authors that the oscillation amplitude is often limited not by the limit cycle amplitude but by feedback mechanisms related to flow reversal in the bottom portion of the channels. However, in this paper, the term "limit cycle" will be loosely employed to describe any asymptotic oscillatory behavior of bounded amplitude.

However, two previous numerical studies—one by Wysocki et al. [6] using the TRACE/PARCS coupled code system [7] and another by Dokhane et al. [8] using the SIMULATE-3K code—indicated a specific tendency towards the rotating pattern under asymptotic limit cycle conditions, for at least some out-of-phase full-core conditions. In these studies, the phase shift between azimuthal modes remained at a constant value (approximately 90°) during the limit cycle, rather than gradually drifting over time as described in the previous paragraph. This was true even for cases where the first two azimuthal modes had different natural frequencies based on linear stability analysis. This suggested that during large-amplitude limit cycle oscillations, the first two azimuthal modes of a BWR do not oscillate independently of each other, as a linear analysis of the neutron flux modes would suggest. Rather, these studies suggest that a nonlinear coupling mechanism between the modes exists which promotes the specific 90° (rotating) behavior.

The primary focus of the current study is to provide further insights into the rotating mode limit cycle behavior from a phenomenological standpoint. To that end, the scope has been narrowed to smaller "N-channel" models including either $N = 2$ or $N = 4$ channels, rather than a full-core model. Primarily, the four-channel model will be used, as this gives the fewest number of channels while still allowing for two separate azimuthal modes (in the coupled case). In addition, a reduced-order model (ROM) is used, which provides a variety of advantages in simplifying the analysis and allowing for ease of physical insights. From this simplified model, insights have been gained into the physical causes for the oscillatory behavior, e.g., rotating versus side-to-side, and these insights may be easily extended for an understanding of the full-core results shown in the previous works.

Numerous previous studies have utilized ROMs to investigate unstable behavior in thermal hydraulic and neutronic systems representative of BWRs. One of the first of these was developed by March-Leuba et al. [9], relying on point kinetics and simplified fuel heat transfer and void reactivity models. However, for the present study, a direct representation of the dynamic fluid mass, momentum, and energy transport behavior was required; thus, the authors selected the ROM by Karve et al. [10] as a starting point; this model includes one of the simplest treatments of the dynamic fluid transport behavior, calculated in a single thermal-hydraulic channel (which was extended to multiple channels in the present work as described below).

Later, Lange [11] and Dokhane [12] were among the first to develop two-channel ROMs which allow for the studying of regional (out of phase) type oscillations in heated and neutronic-coupled channels corresponding to the first azimuthal mode, as well as core-wide oscillations corresponding to the fundamental mode. More recently, Dykin et al. [13] further extended the application of ROMs to four parallel channels, which permit examination of the fundamental mode and the first two azimuthal modes. The work done by Dykin et al. includes investigation of a four-channel case in which all three of these modes are unstable. In the case analyzed, the first two azimuthal models appeared to oscillate independently, with a constantly changing phase shift between these modes. In other words, a specific rotating mode limit cycle behavior was not observed. This is contrary to the findings of the ROM presented in the current work; however, the current work investigates the case of identical TH channels and symmetric neutronic conditions (identical azimuthal modes) while significant asymmetry was present in the model of Dykin et al., which points to the possibility that the azimuthal modes must be sufficiently similar (by some as-yet undetermined criterion) to exhibit the rotating behavior with a fixed phase shift between modes. However, it is also possible that differences in, for example, boundary condition and inlet plenum treatment between the two models could attribute to the difference in behavior as well. However, the authors again point out that the rotating mode behavior was first observed in full-core BWR simulations [13] [6], which indicates that the rotating mode behavior presented in the current work is not purely an artifact of the particular assumptions used for the ROM.

A secondary aim of the current study is to present a new approach for boundary condition treatment in multi-channel systems which, to the authors' knowledge, has not been done previously in quite the same way. This approach freely allows the user to control the preferred oscillation type (in-phase versus out-of-phase) by simple adjustment of inlet and outlet plena loss factors, while maintaining consistency across cases for clear comparison if done properly.

Previous authors have examined, both experimentally and theoretically, the behavior of systems of N identical TH channels connected in parallel via common inlet and outlet plena, in particular when the total flow rate among channels is held constant. For $N = 2$, only the $(0°, 180°)$ pattern is possible (i.e., phase shift of $180°$ between the individual channel oscillations). For $N = 4$, Nakanishi et al. [14] reported experimental results in which two pairs of channels form, with the two channels of each pair oscillating counter-phase to each other but with an arbitrary phase shift for one pair relative to the other. This can be expressed as $(0°, \phi, 180°, 180° + \phi)$, where each element within the parentheses denotes the phase of oscillations in each of the four channels (with the first channel being given a phase of $0°$ by convention) and ϕ is the arbitrary phase shift between the two pairs.

This is sufficient to ensure that the total flow rate remains constant in the linear case (i.e., perfectly sinusoidal oscillations, which occur for small-amplitude oscillations); indeed, as will be shown, examination of the eigenvalues and eigenvectors of the linearized form of the ROM in this paper indicates no preference in the phase shift between counter-oscillating channel pairs. However, for nonlinear oscillations (i.e., oscillations that deviate from simple sinusoidal behavior, as occurs particularly for large-amplitude limit cycle oscillations in BWRs), the total flow rate cannot remain strictly constant and this gives rise to a preference for rotating-mode behavior (at least in terms of thermal hydraulics), as will be demonstrated in this paper.

2. METHODOLOGY

2.1. Reduced-Order Model Description

The ROM used in the present study was introduced by Karve et al. [10] and was selected here as being perhaps the simplest model available which still includes all the elements needed for this study. The original model described consists of a single TH channel with fuel temperature and coolant density feedback provided via a point kinetics model for neutronics. The original model, for a single channel, consists of a system of nine nonlinear ordinary differential equations (ODEs) with the general form

$$\frac{\mathrm{d}\bar{X}(t)}{\mathrm{d}t} = F(\bar{X}(t); \kappa), \tag{2.1}$$

where $\bar{X}(t)$ is the vector of phase variables given by

$$\bar{X}(t) = \left[\mu(t), s(t), v(t), T_{1,1\phi}(t), T_{1,2\phi}(t), T_{2,1\phi}(t), T_{2,2\phi}(t), n(t), c(t)\right]^T, \tag{2.2}$$

and κ is a vector of operating and design parameters. A description of each variable in $\bar{X}(t)$ is given in Table 1. Note that all variables contained in $\bar{X}(t)$ and κ are cast in dimensionless form for all calculations, as described in the original paper [10].

The TH treatment is based on three underlying TH equations, to which a weighted residual method is applied to reduce the three partial differential equations (PDEs) to ODEs. Though higher-order approximations in space can and have been used for ROMs (e.g., by Dokhane [12]), the original Karve model used in this study relies on a first-order approximation in space for each TH variable. Analytical integration is performed separately across the single-phase and two-phase regions of the channel, with the boiling boundary, $\mu(t)$, being solved for as a solution variable. The TH equations are coupled to a fuel

conduction solution based on the method of variations which reduces the heat equation to a set of two ODEs in each region (single- and two-phase regions).

The variable definitions in Table 1 are identical to the phase variables in the original model except that the model has been extended to allow for multiple TH channels in parallel, connected via common inlet and outlet plena. In addition, an option has been added to employ higher-order modal kinetics, up to the first three neutronic modes (i.e., the fundamental and first two azimuthal neutronic modes).

Table 1. Description of phase variables solved for in the model as implemented in the current work

Variable	Description
$\mu_i(t)$	Axial location of boiling boundary for channel i
$s_i(t)$	Slope of quality in two-phase region for channel i
$v_i(t)$	Inlet velocity for channel i
$T_{1,1\phi,i}(t)$	kth expansion coefficient for fuel temperature in single-phase region for channel i
$T_{1,2\phi,i}(t)$	kth expansion coefficient for fuel temperature in two-phase region for channel i
$n_m(t)$	Neutron density for neutronic mode m
$c_m(t)$	Neutron precursor concentration for neutronic mode m

To accomplish these changes, the equations and phase variables governing thermal hydraulics and fuel heat conduction were trivially extended to N channels, with each channel i being solved independently in complete analogy to the original single-channel treatment, with three exceptions: the conduction solution was reduced to a single-region problem (in the radial direction) for simplicity, the inlet and outlet k-factor treatment was altered in a way that was unique to the multi-channel system, and the neutron kinetics treatment was extended from simple point kinetics to multi-modal kinetics, allowing for any number of neutronic modes M as specified by the user. The latter two extensions are described in the following sections.

The resulting system consists of $(5N + 2M)$ nonlinear ODEs, with phase variables given in Table 1, which were solved using MATLAB's built-in *ode23* function, a one-step second-order Runge Kutta method. One additional detail to note in the current implementation was the use of a simple limiter which set any negative values for the phase variables to zero at each solution step, preventing negative solutions which (due to the assumptions inherent in the equations) led to runaway divergence of the solution to infinity in either direction. This proved necessary for the problems shown in this study, as the limit cycles often had large enough amplitudes to give negative velocities during a portion of the oscillation period.

The reader is referred to the original paper by Karve et al. [10] for a detailed description of the underlying fluid and fuel heat conduction equations.

2.2. Boundary Condition Treatment and Inlet Plenum Loss Factors

The behavior of a system of parallel flow channels undergoing oscillations (most commonly, density-wave oscillations) has been the topic of numerous studies, both experimental and analytical. Boundary conditions play an important role in determining the stability characteristics (e.g., whether the in-phase or out-of-phase oscillation mode dominates). For the case of in-phase oscillations, the recirculation loop dynamics play a role, and the boundary conditions may reflect this in terms of additional pressure drop terms or other treatment. However, for the case of out-of-phase oscillations, Grandi et al. [15] have

shown that recirculation loop dynamics play virtually no role at all, and the results are almost identical if one eliminates the recirculation loop dynamics from the model and imposes a constant total core inlet flow rate and a constant core pressure drop boundary condition instead.

More recently, Munoz-Cobo et al. [16] have argued that a constant pressure drop boundary condition should not be imposed along with a constant total mass flow rate condition, as this leads to an overdetermined system of equations and artificially inhibits the variations in total inlet flow rate. Alternately, Dokhane [8] was able to impose a fixed pressure drop boundary condition and still obtain in-phase oscillations, provided that the oscillations remained small in amplitude (1%).

As will be demonstrated in the Results section, applying a fixed pressure drop boundary condition from only the inlet to the outlet of each channel prevents any coupling between channels, at least when neutronics are disabled. In a real BWR, though, the channels are coupled thermal-hydraulically through the inlet and outlet plena, which has a flow rate equal to the sum of the flow rates in all channels at the channel inlet and outlet, respectively. By including a pressure drop term which operates on the total core flow rate, a mechanism is created by which the channels may be coupled to each other. The effects of this extra loss term on the stability characteristics of the system, and the physical reason why it promotes either out-of-phase or in-phase behavior (depending on the values chosen), will be described in detail in the Results section.

In the present work, the pressure loss for the inlet plenum is termed $\Delta P_{below}(t)$ and is applied as a concentrated pressure loss with a local loss factor k_{below} as given by

$$\Delta P_{below}(t) = k_{below}\rho_l v_{inlet,avg}^2(t)\,, \tag{3}$$

where ρ_l is the single-phase liquid density, and $v_{in,avg}(t)$ is the time-dependent average inlet velocity given by

$$v_{inlet,avg}(t) = \frac{1}{N}\sum_{i=1}^{N} v_i(t)\,, \tag{4}$$

where N is the total number of channels and $v_i(t)$ is the inlet velocity for channel i. Likewise, an additional term $\Delta P_{above}(t)$ can be derived based on the average outlet velocity across all channels, properly weighted by channel outlet densities (based on void fraction). This has been done in a more thorough work by Wysocki [17]; however, such an analysis is omitted in the present work, for brevity.

Note that a separate loss term $\Delta P_{inlet,i}(t)$ is still included in the model (as originally implemented by Karve et al.) and operates on the inlet velocity of <u>each channel</u> separately, namely,

$$\Delta P_{inlet,i}(t) = k_{inlet}\rho_l v_i^2(t)\,. \tag{5}$$

Therefore, for example, if one wishes to increase $\Delta P_{below}(t)$ from its default value of 0.0 to some positive value, one may also decrease $\Delta P_{inlet}(t)$ by the same amount in order to maintain precisely the same overall ΔP_{tot} throughout the model, thus maintaining the same steady-state conditions as well. This is an attractive feature which allows for true "apples-to-apples" comparison between cases.

All calculations performed for the ROM were done with MATLAB, including use of the MATLAB Symbolic Toolbox for calculation of eigenvalues and eigenvectors for the linearized system (i.e., the Jacobian) around the steady-state values for the original system of nonlinear ODEs. This was used to provide further insights into the results.

2.3. Multimodal Kinetics

Following the approach used by Dokhane [12], the equations governing the M neutronic modes are given by

$$\frac{\mathrm{d}n_m(t)}{\mathrm{d}t} = \frac{1}{\Lambda}\left[(\rho_m^S - \beta)n_m(t) + \sum_{l=0}^{M-1}\rho_{ml}(t)n_l(t)\right] + \lambda c_m(t), \quad m = 0, M-1 \tag{6}$$

and

$$\frac{\mathrm{d}c_m(t)}{\mathrm{d}t} = \frac{\beta}{\Lambda}n_m(t) - \lambda c_m(t), \qquad m = 0, M-1 \tag{7}$$

where $n_m(t)$ is the amplitude of neutronic mode m, $c_m(t)$ is the precursor concentration for neutronic mode m, ρ_m^S is the static reactivity for mode m (with $\rho_0^S = 0$), and ρ_{ml} is a reactivity term for the coupling between mode m and mode l. Note that only a single energy group is used, which gives the property that the eigenmodes are mutually orthogonal [12].

Again using the notation of Dokhane [12], the reactivity coupling terms are given by

$$\rho_{ml}(t) = \sum_{i=0}^{N} WD_{ml}^{(i)}\left(c_1\Delta\alpha_i(t) + c_2\Delta T_{avg,i}(t)\right), \tag{8}$$

where

$$WD_{ml}^{i} = \frac{\langle\phi_m^*(\vec{r}), \phi_n(\vec{r})\rangle^{(i)}}{\langle\phi_m^*(\vec{r}), \phi_m(\vec{r})\rangle} \text{ and} \tag{9}$$

$$\Delta\alpha_i(t) = [\alpha(t)]_i - \alpha_0. \tag{10}$$

ϕ_m and ϕ_m^* are the shape functions for the static forward and adjoint flux, respectively, of mode m, i is the channel index, and N is the total number of channels. The notation $\langle\cdot\rangle$ denotes spatial integration over the entire domain, while $\langle\cdot\rangle^{(i)}$ denotes integration over the spatial region corresponding to the ith channel only.

For all cases performed in this work, the N channels are always assumed to be identical to each other in terms of geometry and other operating parameters; thus, considering at most four channels, an analogous expression for WD_{ml}^{i} can be written in terms of vector dot products without needing any detailed knowledge of the actual spatial flux shape within each assembly node. For example, for the most complicated case of $N = 4$ and $M = 2$ (four channels and three neutronic modes), one can write

$$\vec{\phi}_0 = \vec{\phi}_0^* = [1, 1, 1, 1]\,, \tag{11}$$

$$\vec{\phi}_1 = \vec{\phi}_1^* = [-1, 1, -1, 1]\,, \tag{12}$$

$$\vec{\phi}_2 = \vec{\phi}_2^* = [-1, -1, 1, 1]\,, \tag{13}$$

and then each term of WD_{ml}^{i} can be calculated using

$$WD_{ml}^{i} = \frac{\phi_{m,i}^*\phi_{l,i}}{(\vec{\phi}_m^*)\cdot(\vec{\phi}_m^*)} = \frac{\phi_{m,i}^*\phi_{l,i}}{4}, \tag{14}$$

where $\phi_{m,i}$ (a scalar) is the ith component of $\vec{\phi}_m$ (i.e., corresponding to channel i). Note that the three vectors $\vec{\phi}_m$ in Eqs. (11)–(13) are mutually orthogonal (as they must be, by definition), and using the channel radial numbering scheme shown in Figure 1, one can visualize Mode 0 as being the fundamental

mode, Mode 1 being the "east-west" mode, and Mode 2 being the "north-south" mode. Note that for 1-mode, 1-channel problems, $\vec{\phi}_0 = \vec{\phi}_0^* = [1]$, while for 2-mode, 2-channel problems, $\vec{\phi}_0 = \vec{\phi}_0^* = [1, 1]$ and $\vec{\phi}_1 = \vec{\phi}_1^* = [-1, 1]$.

1	2
3	4

Figure 1.Channel radial numbering scheme for the coupled four-channel problem.

2.4. Linearized versus Nonlinear Analyses

In general, BWRs behave nonlinearly, with significant nonlinearities present in the underlying equations themselves (i.e., the neutron kinetics equations and the two-phase mass-momentum-energy fluid equations) as well as in the coupling between the neutronics and TH fields expressed through nonlinear feedback terms. However, while the behavior of a BWR is nonlinear in general, the system will behave linearly in the neighborhood of a hyperbolic fixed point. In other words, the stability of the system may be described by linearized forms of the governing equations provided that the deviation from steady-state conditions remains sufficiently small.

The linearized system can be written as a series of first-order, homogeneous* ordinary differential equations about the fixed point of the form

$$\frac{d\left(\underline{x}(t)\right)}{dt} = \frac{d\left(\delta\underline{x}(t)\right)}{dt} = \underline{\underline{A}}\,\delta\underline{x}(t)\,, \tag{2.15}$$

where $\underline{x}(t)$ is the solution vector containing the entire problem domain (i.e., all variables for all spatial nodes), $\delta\underline{x}(t)$ is the deviation of $\underline{x}(t)$ from the fixed point $\underline{x}_0$ (i.e., $\delta\underline{x}(t) = \underline{x}(t) - \underline{x}_0$), and the matrix $\underline{\underline{A}}$ is the Jacobian matrix containing the linear (i.e., first derivative) coefficients for the entries in $\underline{x}(t)$ about the point $\underline{x}_0$. Using the relation

$$\underline{\underline{A}}\,\underline{v}_n = \lambda_n \underline{v}_n, \tag{2.16}$$

where $\underline{v}_n$ is any eigenvector of $\underline{\underline{A}}$, with a corresponding eigenvalue of λ_n, it can be shown by inspection that

$$\delta\underline{x}(t) = \sum_{n=1}^{\infty} c_n e^{\lambda_n t}\underline{v}_n \tag{2.17}$$

is a solution of Eq. (2.15).

For the general case of complex eigenvalues, it is useful to rewrite Eq. (2.17) as

$$\delta\underline{x}(t) = \sum_{n=1}^{\infty} c_n e^{\gamma_n t}\left(\cos(\omega_n t) + i\sin(\omega_n t)\right)\underline{v}_n\,, \tag{2.18}$$

where γ_n and ω_n are the real and imaginary components of the eigenvalue λ_n, respectively. If λ_n contains an imaginary component, then at least some of the elements of v_n must contain imaginary components as well, in order to satisfy Eq. (2.16). Furthermore, as imaginary eigenvalues must occur in conjugate pairs, the corresponding eigenvectors must occur in conjugate pairs as well, given that the coefficients of $\underline{\underline{A}}$ are all real [19], as is the case here. Assuming that two modes k and k^* form a conjugate pair, the two corresponding $n = k$ and $n = k^*$ terms in Eq. (2.18) can be rewritten with real coefficients as

* In the absence of external sources (e.g., neutron sources)

$$c_k e^{\gamma_k t}\left(\cos(\omega_k t)\underline{v}_{k,r} - \sin(\omega_k t)\underline{v}_{k,i}\right)$$

and

$$c_k e^{\gamma_k t}\left(\cos(\omega_k t)\underline{v}_{k,i} + \sin(\omega_k t)\underline{v}_{k,r}\right),$$

where $\underline{v}_{k,r}$ and $\underline{v}_{k,i}$ are the real and imaginary components of $\underline{v}_k$, respectively. Thus, when converted to the real domain, the two modes exhibit the same exponential coefficient but with different combinations of spatial vectors weighted by sinusoidal time-dependent components.

Note that if λ_n is a real number, $\omega_n = 0$ and the expression reduces to Eq. (2.17) with λ_n replaced by γ_n. Hence, regardless of the complexity of λ_n, if $\gamma_n > 0$, the nth component will grow unbounded for $\gamma_n > 0$ but will approach zero for $\gamma_n < 0$, either as a simple exponential or as a growing (or decaying) sinusoid if λ_n is real or complex, respectively.

From here on, according to convention, the eigenvalues and eigenvectors will be sorted in order of decreasing real component; i.e.,

$$\gamma_0 \geq \gamma_1 \geq \gamma_2 \geq \cdots \geq \gamma_{n-1} \geq \gamma_n \geq \cdots \tag{2.19}$$

for all $n > 0$.

From Eq. (2.18) it follows that, after a sufficiently long time, the term corresponding to the largest value of γ_n (i.e. γ_0) will dominate the time-dependent response, as all other terms decay away at a faster rate or grow at a slower rate than this term. This is true for the linearized system of equations; however, numerous numerical studies in the literature have found that the limit cycle behavior is characterized by this consideration of the linearized eigenvalues as well, at least in terms of whether the limit cycle oscillates in-phase or out-of-phase.

2.5. Calculation of Phase Shifts

To find the phase shift values, a subroutine was used which finds all points for each channel velocity (or mass flow rate) signal where the velocity crosses from below the steady state value to above that value (linearly interpolating the nearest two timestep points in the signal), then comparing that "crossover point" to the most recent crossover point for Channel 1, finding the time difference as a fraction of the total oscillation period, then multiplying by 360 degrees to find the phase shift value at that point in time. For example, if the Channel 2 time value was halfway between the two nearest Channel 1 values, the Channel 2 phase shift would be calculated as 180°; but if the Channel 2 value was one-quarter of the way between the previous and subsequent time values, the Channel 2 phase shift would be 90° and so on (the Channel 1 phase shift is always reported as 0°, by convention). All such phase shift values, for all channels, were then plotted consecutively with time on the x-axis and phase shift on the y-axis.

3. RESULTS

3.1. Steady-State Solution

Table 2 shows the steady-state values calculated for the single-channel model, named Case C-1A, with $N_{sub} = 1.5$ and $\tilde{n} = 1.69$. These values correspond exactly to the values calculated by Karve et al. [10] for the same conditions. The leading eigenvalue for this case was found to belong to the complex pair $0.263 \pm 7.840i$, which in the time domain corresponds to a growing exponential based on the real part multiplied by a sinusoidal oscillation with frequency based on the complex part.

Table 2. Steady-state values for all phase variables in all channels, across all cases shown in this paper, for $N_{sub} = 1.5$

Variable	Steady-state value
$\tilde{\mu}$	0.231
$\tilde{s}$	0.350
$\tilde{v}$	0.878
$\tilde{n}$	1.69
$\tilde{c}$	2957

However, initially, stand-alone TH cases were desired; to accomplish this, all parameters were kept the same (including $\tilde{n}$) except that the feedback reactivity coefficients c_1 and c_2 in the model (corresponding to void and fuel temperature feedback, respectively) were reduced from their original values of -0.15 and $-2.0x10^{-5}$, respectively (in nondimensional terms), to $c_1 = c_2 = 0.0$. Thus, changes in void fraction and fuel temperature have no effect on the reactivity terms, so that the power levels (and therefore the heat reaching the coolant) remain constant, acting as a fixed-heat-flux boundary condition typical of stand-alone TH problems.

This, however, decreased the oscillatory eigenvalue pair from $0.263 \pm 7.840i$ to $-4.275 \pm 5.852i$, bringing the operating point far within the stable region, due to the loss of the neutronic feedback which has a destabilizing effect. To compensate, the values of k_{inlet} and k_{outlet} in the TH momentum equation were adjusted to bring the stand-alone TH case back to slightly unstable conditions. In the original model by Karve et al., values of $k_{inlet} = 15$ and $k_{outlet} = 2.5$ were given; for stand-alone TH cases in the current study, values of $k_{inlet} = 2.8$ and $k_{outlet} = 6.0$ were chosen instead. This decreased the single- to two-phase pressure drop ratio, which decreased the stability of the system. The methodology for choosing these values was based on maintaining the same ΔP_{tot} across the model while also giving the desired real eigenvalue component; further details are given in a separate work [17].

3.2. Stand-alone TH Results

One-Channel Results

A one-channel stand-alone TH case, Case S-1A, was performed primarily for comparison to the two- and four-channel cases. Table 3 lists the eigenvalues determined from the steady-state solution for this case. Note that for this case, $k_{inlet} = 2.8$, while k_{below} has no practical meaning and was set to 0.0. Recall from Section 2.4 that the complex eigenvalue pair $0.331 \pm 8.277i$ corresponds to the unstable oscillatory mode, with the positive real component indicating a positive (unstable) oscillation growth rate and the imaginary component corresponding to the oscillation frequency (i.e., $\gamma_0 = 0.331$ and $\omega_0 = 8.277$).

Table 3. Eigenvalues for the single-channel stand-alone TH case (Case S-1A) with $k_{inlet} = 2.8$

Eigenvalue
0.330+8.277i
0.330-8.277i
0.000
-0.300
-0.315
-47.211
-199.889

Two-Channel Results

Two different two-channel stand-alone TH cases were run: Case S-2A, using values of $k_{inlet} = 2.8$ and $k_{below} = 0.0$, and Case S-2B, using values of $k_{inlet} = 1.8$, and $k_{below} = 1.0$. Eigenvalues and corresponding eigenvector shapes are shown in Table 4. The eigenvector shapes (i.e., in-phase, out-of-phase, or arbitrary phase shift) were determined by direct examination of the eigenvectors. Time-dependent channel inlet velocity values as well as the phase shift between the velocity oscillations in each channel are shown in Figure 2 and Figure 3.

Note that the eigenvalues for Case S-2A are identical to those for Case S-1A, except that each eigenvalue is repeated. Each of these eigenvalue pairs is degenerate, meaning that each of the two eigenvectors in each pair corresponds to oscillatory behavior in one of the two channels, or linear combinations thereof. The key point is that the two channels oscillate independently, as the oscillatory eigenvalues ($0.330 \pm 8.277i$) are applicable to any arbitrary phase shift between the channel oscillations. This independent behavior between channels was confirmed by applying various initial conditions to each channel and confirming that the asymptotic phase shift between the channels was strictly dependent on initial conditions.

This independent behavior occurs because the fixed ΔP_{tot} boundary condition is applied to each channel separately, with all ΔP terms operating on individual channel parameters only. In order to obtain a distinct in-phase or out-of-phase characteristic behavior, the k_{below} term must be nonzero (based on how the boundary conditions are set up in the ROM). This is seen in Case S-2B (Figure 3), which shows a clear evolution towards out-of-phase oscillation (i.e., $180°$ phase shift between channels), regardless of initial conditions. This is represented also in Table 4, which indicates that one complex eigenvalue pair still exists at the same value of $0.330 \pm 8.277i$, but now the other pair exists at $0.843 \pm 8.290i$ instead. Inspection of the corresponding eigenvector reveals that this corresponds to an out-of-phase oscillation case ($180°$ phase shift between channels), while the $0.330 \pm 8.277i$ now corresponds specifically to in-phase oscillations ($0°$ phase shift).

Table 4. Eigenvalues and corresponding oscillation types for the two-channel stand-alone TH case with $k_{inlet} = 2.8$ and $k_{below} = 0.0$ (Case S-2A) or with $k_{inlet} = 1.8$ and $k_{below} = 1.0$ (Case S-2B)

Case S-2A		Case S-2B	
Eigenvalue	**Oscillation Type**	**Eigenvalue**	**Oscillation Type**
0.330+8.277i	Arbitrary	0.843-8.290i	Out-of-phase
0.330+8.277i	Arbitrary	0.843+8.290i	Out-of-phase
0.330-8.277i	Arbitrary	0.330+8.277i	In-phase
0.330-8.277i	Arbitrary	0.330-8.277i	In-phase
0.000	-	0.000	-
0.000	-	0.000	-
-0.300	-	-0.300	-
-0.300	-	-0.300	-
-0.315	-	-0.315	-
-0.315	-	-0.315	-
-47.211	-	-44.772	-
-47.211	-	-47.211	-
-199.889	-	-199.889	-
-199.889	-	-199.889	-

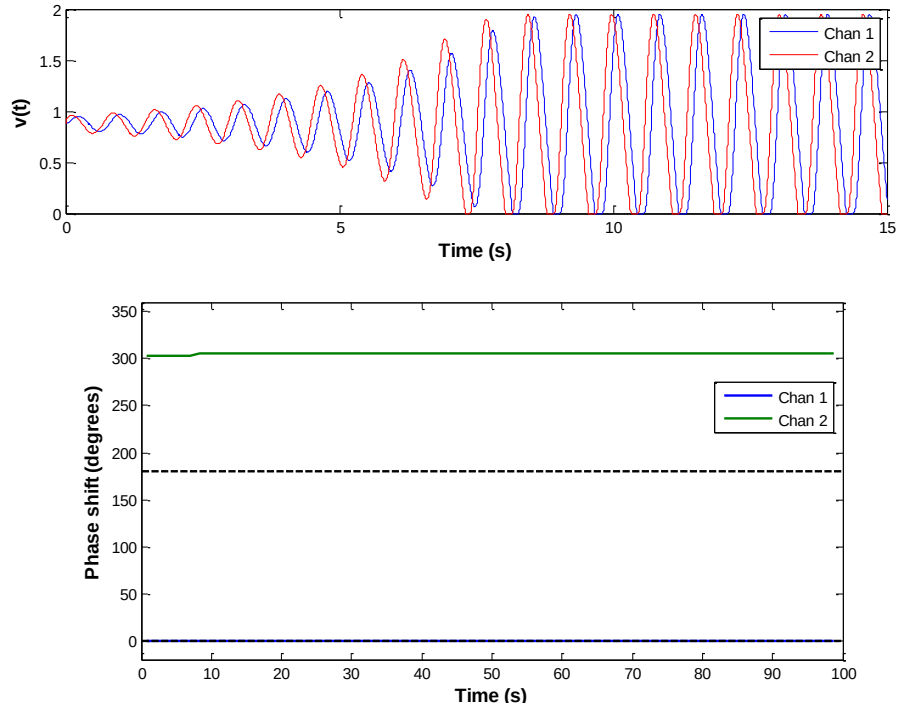

Figure 2. Inlet velocity $v_i(t)$ for each channel i (top) and evolution over time of the phase shift of each channel relative to Channel 1 (bottom), for the two-channel stand-alone TH case with $k_{inlet} = 2.8$ and $k_{below} = 0.0$ (Case S-2A).

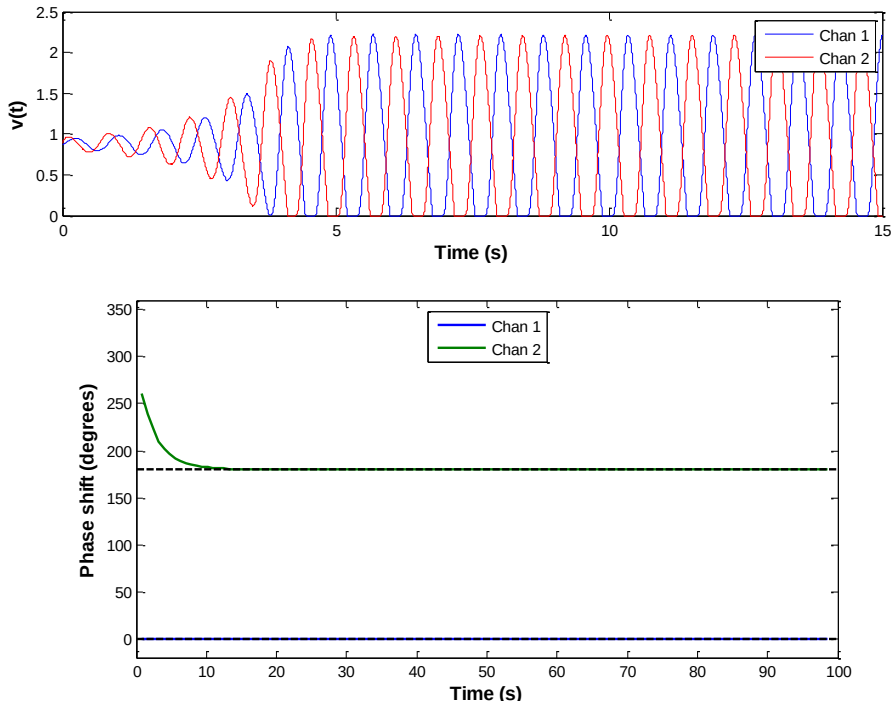

Figure 3. Inlet velocity $v_i(t)$ for each channel i (top) and evolution over time of the phase shift of each channel relative to Channel 1 (bottom), for the two-channel stand-alone TH case with $k_{inlet} = 1.8$ and $k_{below} = 1.0$ (Case S-2B).

The physical reason for this behavior in Case S-2B is as follows. In the in-phase oscillation case, the average inlet velocity ($v_{inlet,avg}(t)$ in Eq. (3)) oscillates identically to $v_1(t)$ and $v_2(t)$ (the individual channel velocities). Thus, the in-phase oscillation mode exhibits the exact same behavior as if two channels were independent (as in Case S-2A) or as in a corresponding single-channel case if it were performed instead. However, in the out-of-phase oscillation case, $v_{inlet,avg}(t)$ no longer oscillates the same as $v_1(t)$ and $v_2(t)$; in fact, $v_{inlet,avg}(t)$ is constant in time since the oscillation in Channel 1 cancels out the oscillation in Channel 2, at least for linear oscillations (for nonlinear oscillations with additional Fourier frequency components, the average flow cannot in general be strictly constant). This means that $\Delta P_{below}(t)$ remains constant in time, meaning that each channel is effectively oscillating at a reduced total ΔP (since the contribution normally associated with $\Delta P_{below}(t)$ no longer "participates" in the oscillations).

More specifically, the effective pressure drop in the single-phase region is reduced (in terms of what oscillates), meaning that the effective two-phase to single-phase pressure drop ratio is increased. This, as is well known in the study of density-wave oscillations, has a destabilizing effect on the system, accounting for the increased real eigenvalue component of the out-of-phase mode shown in Table 4.

It is worthwhile to note that additional cases were performed by Wysocki [17], finding that the addition of an outlet plenum loss factor k_{above} had the opposite effect, promoting the in-phase mode over the out-of-phase mode, for the reverse reasoning as given above.* In this case, the in-phase mode still had an

* Furthermore, a negative value of k_{below} (or negative k_{above}) promoted the in-phase mode (or out-of-phase mode, respectively) as well, although the use of negative loss factors was purely academic and not physical.

eigenvalue of $0.330 \pm 8.277i$ while the out-of-phase mode had an eigenvalue with a real component less than 0.330, which can be understood based on the discussion above.

Four-Channel Results

Two four-channel cases were performed: Case S-4A (analogous to Case S-2A), with $k_{below} = 0.0$ and $k_{inlet} = 2.8$, and Case S-4B (analogous to Case S-2B), with $k_{below} = 1.0$ and $k_{inlet} = 1.8$. Eigenvalues are shown in Table 5. The eigenvalues (and eigenvectors) were simply repeats of the corresponding two-channel values except with four complex pairs. In Case S-4A, as expected, all four complex eigenvalue pairs were degenerate, and the phase shift between channels was once again arbitrary.

In Case S-4B, one complex eigenvalue pair was the in-phase $0.330 \pm 8.277i$ pair and the other three were degenerate $0.843 \pm 8.290i$ complex pairs. This degeneracy is expected, as the increased number of channels introduced additional "degrees of freedom" in which the channels could oscillate out-of-phase in different combinations and still maintain a constant total inlet velocity (at least for the case of linear oscillations). By examination of the eigenvectors, this degeneracy manifests itself as two channels oscillating 180° counter-phase and the other two channels oscillating 180° counter-phase, with an arbitrary (i.e., degenerate) phase shift between each pair of channels.

Table 5. Leading eigenvalues (with the largest real components) and corresponding oscillation types for the four-channel stand-alone TH case with $k_{inlet} = 2.8$ and $k_{below} = 0.0$ (Case S-4A), or with $k_{inlet} = 1.8$ and $k_{below} = 1.0$ (Case S-4B)

Case S-4A		Case S-4B	
Eigenvalue	**Oscillation Type**	**Eigenvalue**	**Oscillation Type**
0.330+8.277i	Arbitrary	0.843-8.290i	Out-of-phase
0.330+8.277i	Arbitrary	0.843-8.290i	Out-of-phase
0.330+8.277i	Arbitrary	0.843-8.290i	Out-of-phase
0.330+8.277i	Arbitrary	0.843+8.290i	Out-of-phase
0.330-8.277i	Arbitrary	0.843+8.290i	Out-of-phase
0.330-8.277i	Arbitrary	0.843+8.290i	Out-of-phase
0.330-8.277i	Arbitrary	0.330-8.277i	In-phase
0.330-8.277i	Arbitrary	0.330-8.277i	In-phase
0.000	-	0.000	-
0.000	-	0.000	-
0.000	-	0.000	-
0.000	-	0.000	-
-0.300	-	-0.300	-
-0.300	-	-0.300	-
-0.300	-	-0.300	-
-0.300	-	-0.300	-

Eigenvalue	Oscillation Type
0.843+8.290i	Out-of-phase
0.843+8.290i	Out-of-phase
0.843+8.290i	Out-of-phase
0.843-8.290i	Out-of-phase
0.843-8.290i	Out-of-phase
0.843-8.290i	Out-of-phase
0.330+8.277i	In-phase
0.330-8.277i	In-phase
0.000	-
0.000	-
0.000	-
-0.300	-
-0.300	-
-0.300	-
-0.300	-

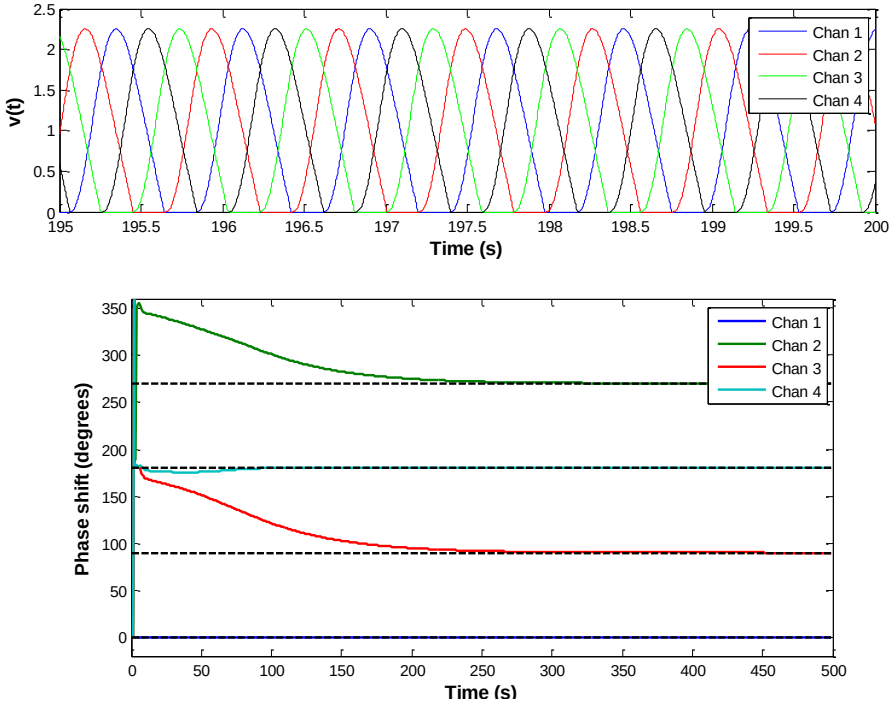

Figure 4. Inlet velocity $v_i(t)$ for each channel i (top) and evolution over time of the phase shift of each channel relative to Channel 1 (bottom), for the four-channel stand-alone TH case with $k_{inlet} = 1.8$ and $k_{below} = 1.0$ (Case S-4B).

This is confirmed by the time-dependent simulation results shown in Figure 4, particularly the phase plot which shows Channels 1 and 4 quickly forming into a 180° pair, and Channels 2 and 3 forming a separate 180° pair, occurring by about 10 seconds into the simulation and continuing indefinitely. (Channel 1 could have instead formed a pair with Channel 2 or with Channel 3, depending on initial conditions.)

However, the key finding, which is not possible to observe in the linear eigenvalue analysis, is that the value of ϕ gradually moves towards $90.00°$ and remains there asymptotically; in other words, the four-channel model specifically favors the $(0°, 90°, 180°, 270°)$ oscillation pattern (to an arbitrary number of decimal places over time). This oscillation pattern naturally corresponds to a "rotating mode" behavior, except that the actual ordering of the channels is arbitrary for the stand-alone TH case. For the coupled case, the ordering is no longer arbitrary, and the behavior even more closely resembles that of the full-core rotating mode system, as will be shown in the next section.

3.3. Coupled Results

This section describes results for the coupled neutronic-TH cases, which used the radial channel numbering scheme shown in Figure 1. In these cases, the reactivity coefficients c_1 and c_2 were increased from 0.0 (stand-alone TH) to some fraction of their nominal values. First, with $c_1 = c_2 = 0.0$, the k_{inlet} and k_{outlet} values were returned to their nominal values of 15.0 and 2.5, respectively; then, k_{below} was increased until the out-of-phase modes had a real component of 1.000 (chosen arbitrarily, to yield sufficiently unstable results for quicker limit cycle evolution). Additional cases, shown in Table 6, were performed by incrementally decreasing k_{below} from this value and increasing c_1 and c_2 by the same fraction of their nominal amounts in order to maintain the same real component of 1.000 in the out-of-phase mode for consistency across all cases.

Table 6. Final limit cycle phase shift depending on the relative strength of neutronic versus TH channel coupling*

			Final Limit Cycle Phase Shift (degrees)			
Case	k_{below}	c_1, c_2 Multiplier	Chan. 1	Chan. 2	Chan. 3	Chan. 4
C-4A	11.000	0.388	0.0	0.0	180.0	180.0
C-4B	11.500	0.336	0.0	0.0	180.0	180.0
C-4C	11.750	0.310	0.0	0.0	180.0	180.0
C-4D	11.875	0.297	0.0	329.6	149.6	180.0
C-4E	12.000	0.284	0.0	318.1	138.1	180.0
C-4F	12.125	0.271	0.0	305.8	125.8	180.0
C-4G	12.250	0.258	0.0	270.0	90.0	180.0
C-4H	12.500	0.231	0.0	270.0	90.0	180.0
C-4I	13.000	0.177	0.0	270.0	90.0	180.0
C-4J	13.500	0.121	0.0	270.0	90.0	180.0

* The real component of the out-of-phase eigenvalue pair was 1.00000 in each case, the value of $\boldsymbol{k_{inlet}}$ was set to $(\mathbf{15.0} - \boldsymbol{k_{below}})$ in each case to maintain a constant total $\Delta \boldsymbol{P}$, and the steady-state solution was the same across all cases (as given in **Table 2**).

Thus, a series of cases was created that had a progressively stronger neutronic coupling between channels (via the reactivity coefficients c_1 and c_2) and a progressively weaker TH coupling between channels (via the inlet plenum loss coefficient k_{below}). Results for the final limit cycle phase shift pattern for each case are shown in Table 6 as well, with the phase shift plot examined visually in each case to ensure convergence (or run for a longer time if not). Phase shift as a function of time is shown in Figure 5 as well, for three select cases.

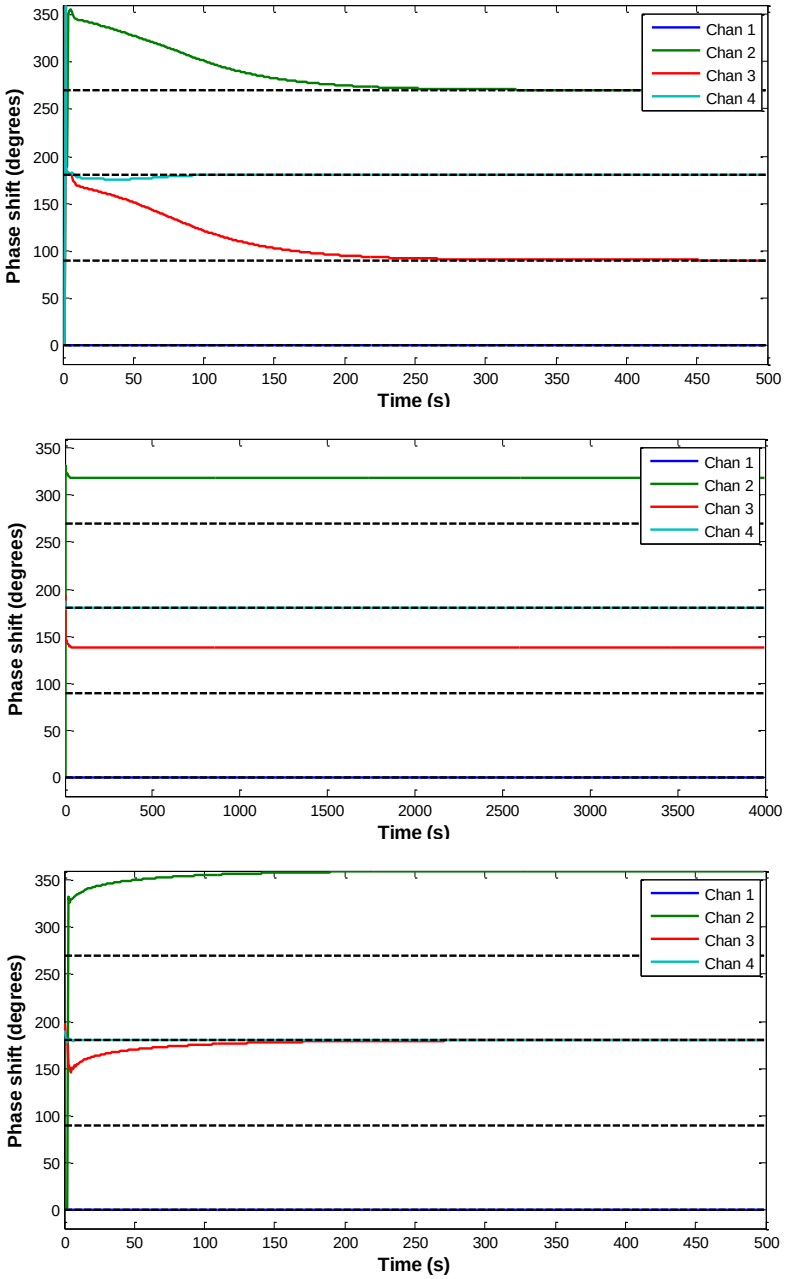

Figure 5. Evolution over time of the phase shift of each channel relative to Channel 1, for the coupled four-channel cases C-4G (top), C-4E (middle), and C-4C (bottom).

The results show the following clear trend: cases with relatively stronger TH channel coupling favor the rotating mode behavior, while cases with relatively stronger neutronic channel coupling favor the side-to-side mode. Note that the channel ordering is no longer arbitrary: in the rotating case, the phase shifts are arranged in a counterclockwise order (i.e., Channels 1-3-4-2), while clockwise (Channels 1-2-4-3) was also observed to occur in other simulations (not shown), but no other channel ordering was observed for any set of initial conditions. This is understandable based on the spatial channel coupling created by the modal neutronics equations.

Additionally, an interesting "transition region" exists in the calculated results, in which the final, converged limit cycle behavior is established at some intermediate phase shift somewhere between rotating and side-to-side. The cause for this "transition" behavior is not known at this time.

It is possible that the findings in this section in terms of favoring side-to-side or rotating behaviors could be influenced by certain assumptions or approximations made in the reduced order model, such as neglecting the delayed feedback reactivities and assuming that the neutron generation time Λ in Eqs. (6) and (7) is time same for all modes (which allows eliminating some of the coupling terms between modes; see Dokhane [12] for further discussion). More detailed investigation of the impact of such assumptions on the observed out-of-phase oscillation behavior is left as a topic of future investigation.

As explained earlier in this paper, it is well understood that the neutronic feedback favors the in-phase oscillation mode over the out-of-phase mode, due to the subcriticality of the out-of-phase neutron flux harmonics. Likewise, the TH field favors the out-of-phase mode due to boundary condition effects (explained above) or, similarly, recirculation loop dynamics. This leads to the conclusion that the same conditions which favor the out-of-phase mode (i.e., relatively strong TH channel coupling and weak neutronic coupling) also favor the rotating-mode behavior. Therefore, it seems plausible that the most likely out-of-phase limit cycle behavior for full-core BWRs is the rotating mode; if the neutronic coupling were sufficiently strong, then the in-phase mode would occur rather than the side-to-side out-of-phase behavior. This conjecture requires further examination with full-core BWR models, however.

4. CONCLUSIONS

The results of this study suggest the existence of a preferred "rotating mode" behavior using a reduced-order model with four TH channels connected by a common inlet plenum. This behavior was found for all four-channel stand-alone TH simulations performed with the ROM. A follow-up study will provide a physical explanation for why the rotating mode is preferred over the side-to-side or other out-of-phase oscillatory behaviors, for cases with stand-alone TH or with weak neutronic coupling.

For the case of coupled TH/neutronics, results indicate that the side-to-side mode is preferred for sufficiently strong neutronic feedback (i.e., sufficiently large reactivity feedback coefficients). The reason for the neutronic mode favoring the side-to-side oscillatory behavior is also left as a topic for further investigation. However, it was noted that strong neutronic feedback also favors the in-phase mode, which suggests that the side-to-side out-of-phase limit cycle behavior might only occur in a narrow band of system conditions, while the most likely behavior for out-of-phase oscillations might be the rotating mode. Further study is required to examine this conjecture, though.

The present study investigated only the special case where all channels were hydraulically identical and perfect radial symmetry existed in the neutronic configuration. Additional study is needed to investigate the previous finding by Wysocki et al. [6] that the rotating mode is preferred in at least some cases when the first two azimuthal modes have different eigenvalues and natural frequencies. Bifurcation analyses may be used in future analyses to develop a more complete understanding of the phenomena laid out in this paper as well.

This paper also presented a novel approach to understanding in-phase versus out-of-phase oscillations in systems of parallel TH channels, in terms of the application of inlet and outlet boundary conditions and their connection to the eigenvalues of the system about the steady-state fixed point solution. A follow-up study will build upon this understanding by relating it to the case of rotating versus side-to-side oscillations as well.

5. REFERENCES

[1] J. March-Leuba and J. M. Rey, "Coupled thermohydraulic-neutronic instabilities in boiling water reactors: a review of the state of the art," *Nucl. Eng. Des.*, vol. 145, pp. 97-111, 1993.

[2] J. Blomstrand, "The KKL core stability test, conducted in September 1990," ABB-Report BR91-245, 1992.

[3] S. Andersson and M. Stepniewski, "RAMONA-3B calculations of core-wide and regional power/flow oscillations - comparison with Oskarshamn 3 natural circulation test data," in *Proceedings of the OECD/CSNI International Workshop on Boiling Water Reactor Stability, sponsored by the Nuclear Energy Agency of the Organisation for Economic Cooperation and Development*, Holtsville, NY, 1990.

[4] R. Miro, D. Ginestar, D. Hennig and G. Verdu, "On the regional oscillation phenomenon in BWR's," *Prog. Nucl. Energ.*, vol. 36, no. 2, pp. 189-229, 2000.

[5] F. Zinzani, C. Demaziere and C. Sunde, "Calculation of the eigenfunctions of the two-group neutron diffusion equation and application to modal decomposition of BWR instabilities," *Ann. Nucl. Energy*, vol. 35, pp. 2109-2125, 2008.

[6] A. Wysocki, J. March-Leuba, A. Manera and T. Downar, "TRACE/PARCS analysis of out-of-phase power oscillations with a rotating line of symmetry," *Ann. Nucl. Energy*, vol. 67, pp. 59-69, 2014.

[7] U.S. NRC, "TRACE V5.0P3 Theory Manual: Field Equations, Solution Methods, and Physical Models," Division of Safety Analysis, Office of Nuclear Regulatory Research, Washington, DC, 2012.

[8] A. Dokhane, H. Ferroukhi and A. Pautz, "On out-of-phase higher mode oscillations with rotation and oscillation of symmetry line using an advanced integral stability methodology," *Ann. Nucl. Energy*, vol. 67, pp. 21-30, 2013.

[9] J. March-Leuba, D. G. Cacuci and R. B. Perez, "Nonlinear dynamics and stability of boiling water reactors: Part 1 - Qualitative analysis," *Nucl. Sci. Eng.*, vol. 93, pp. 111-123, 1986.

[10] A. A. Karve, Rizwan-uddin and J. J. Dorning, "Stability analysis of BWR nuclear coupled thermal-hydraulics using a simple model," *Nucl. Eng. Des.*, vol. 177, pp. 155-177, 1997.

[11] C. Lange, "Advanced nonlinear stability analysis of boiling water nuclear reactors," Ph.D. thesis. Technical University of Dresden.

[12] A. Dokhane, "BWR stability and bifurcation analysis using a novel reduced order model and the system code RAMONA," Doctoral thesis. École polytechnique fédérale de Lausanne, Lausanne, Switzerland, 2004.

[13] V. Dykin, C. Demaziere, C. Lange and D. Hennig, "Investigation of global and regional BWR instabilities with a four heated-channel Reduced Order Model," *Annals of Nuclear Energy*, vol. 53, pp. 381-400, 2013.

[14] S. Nakanishi, M. Ozawa and S. Ishigai, "The Modes of Flow Oscillation in Multi-Channel Two-Phase Flow Systems," in *Advances in Two-Phase Flow and Heat Transfer*, vol. II, S. Kakac and M. Ishii, Eds., Boston, Martinus Nijhoff Publishers, 1983, pp. 709-724.

[15] G. M. Grandi and K. S. Smith, "BWR stability analysis with SIMULATE-3K," in *Proc. of International Conference on the New Frontiers of Nuclear Technology Safety and High Performance Computing (PHYSOR-2002)*, Seoul, Korea, 2002.

[16] J. L. Munoz-Cobo, M. Z. Podowski and S. Chiva, "Parallel channel instabilities in boiling water reactor systems: boundary conditions for out of phase oscillations," *Ann. Nucl. Energy*, vol. 29, pp. 1891-1917, 2002.

[17] A. Wysocki, "Investigation of limit-cycle behavior in BWRs with time-domain analysis," Ph.D. Thesis. University of Michigan, Ann Arbor, MI, 2015.

[18] J. Guckenheimer and P. Holmes, Nonlinear oscillations, dynamical systems and bifurcations of vector fields, New York: Springer Verlag, 1983.

[19] D. G. Zill and M. R. Cullen, Advanced Engineering Mathematics, Sudbury, MA: Jones and Bartlett Publishers, 2006.

[20] J. L. Munoz-Cobo and G. Verdu, "Application of Hopf bifurcation theory and variational methods to the study of limit cycles in boiling water reactors," *An. Nuc. En.*, vol. 18, no. 5, pp. 269-302, 1991.

[21] M. Tsuji, K. Nishio and M. Narita, "Stability analysis of BWRs using bifurcation theory," *J. Nucl. Sci. Technol.*, vol. 30, no. 11, pp. 1107-1119, 1993.

APPENDIX

Figure 6 through Figure 11 show detailed time-dependent results for the coupled ROM cases presented in Section 3.1.3. The results of these figures correspond to the phase shifts shown in Figure 5.

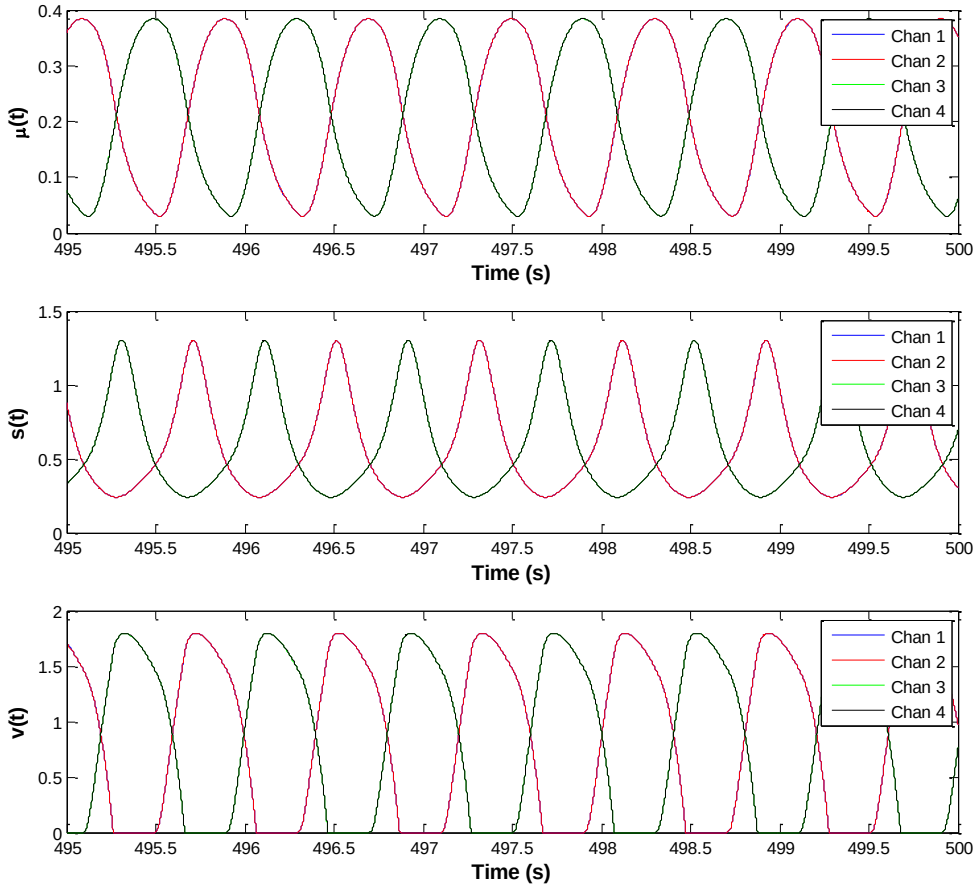

Figure 6. Fully converged limit cycle results for Case C-4C (TH variables). In all three figures, the Chan 1 and Chan 2 lines overlap, and the Chan 3 and Chan 4 lines overlap.

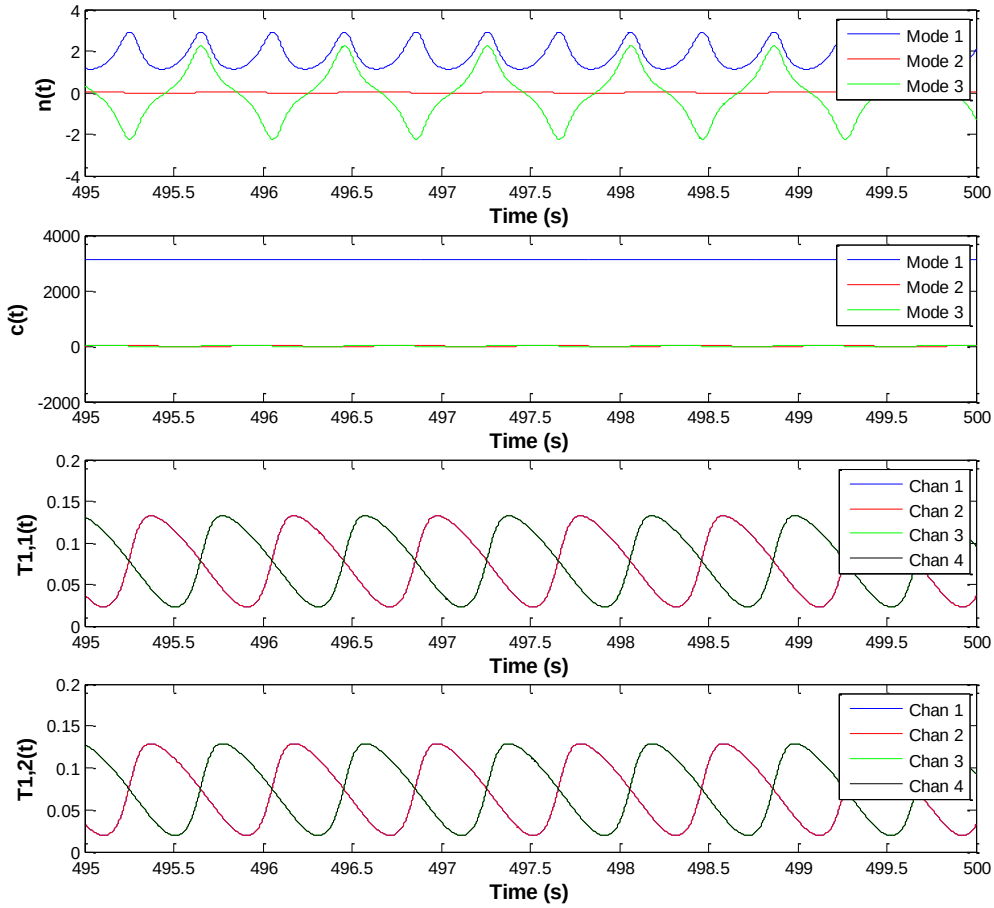

Figure 7. Fully converged limit cycle results for Case C-4C (neutronic variables). In the bottom two figures, the Chan 1 and Chan 2 lines overlap, and the Chan 3 and Chan 4 lines overlap.

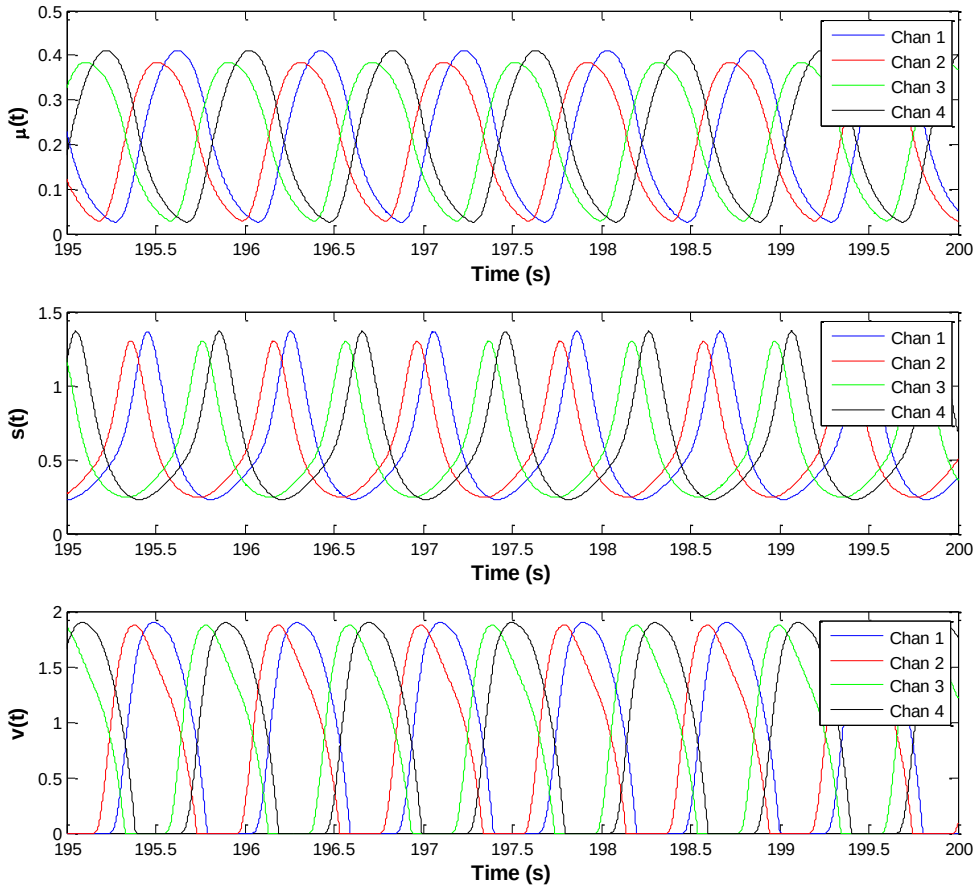

Figure 8. Fully converged limit cycle results for Case C-4E (TH variables).

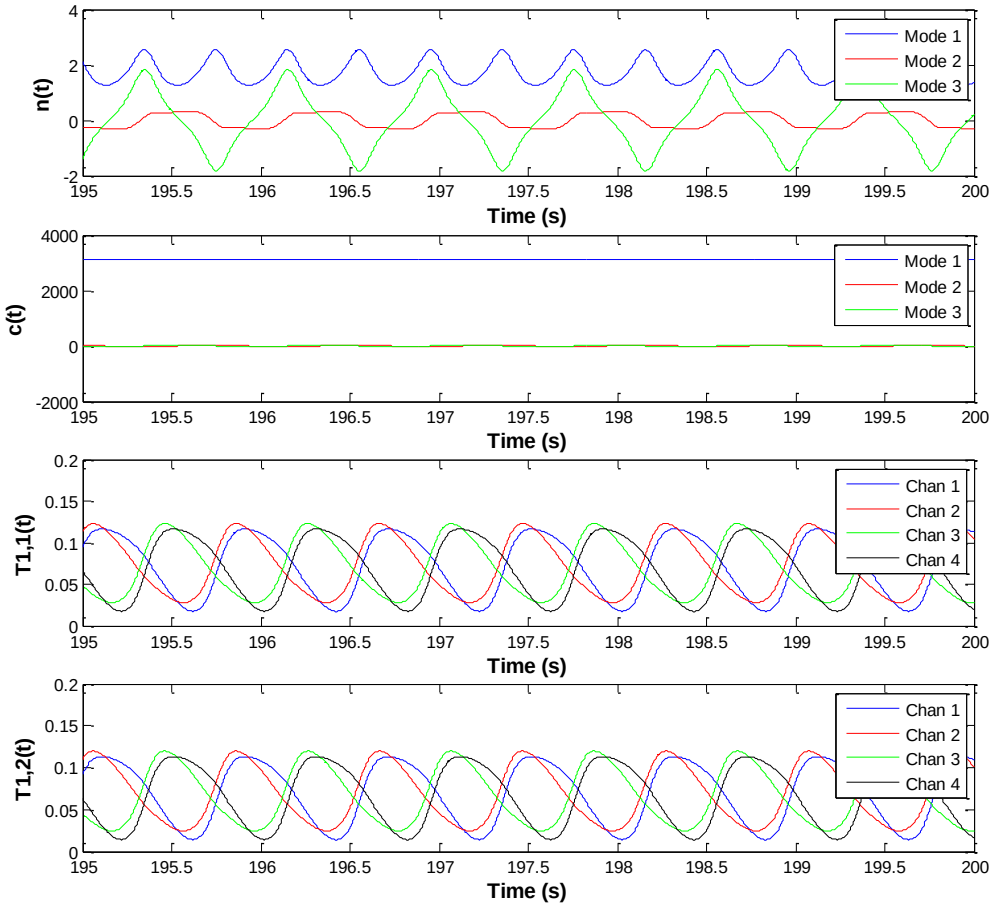

Figure 9. Fully converged limit cycle results for Case C-4E (neutronic variables).

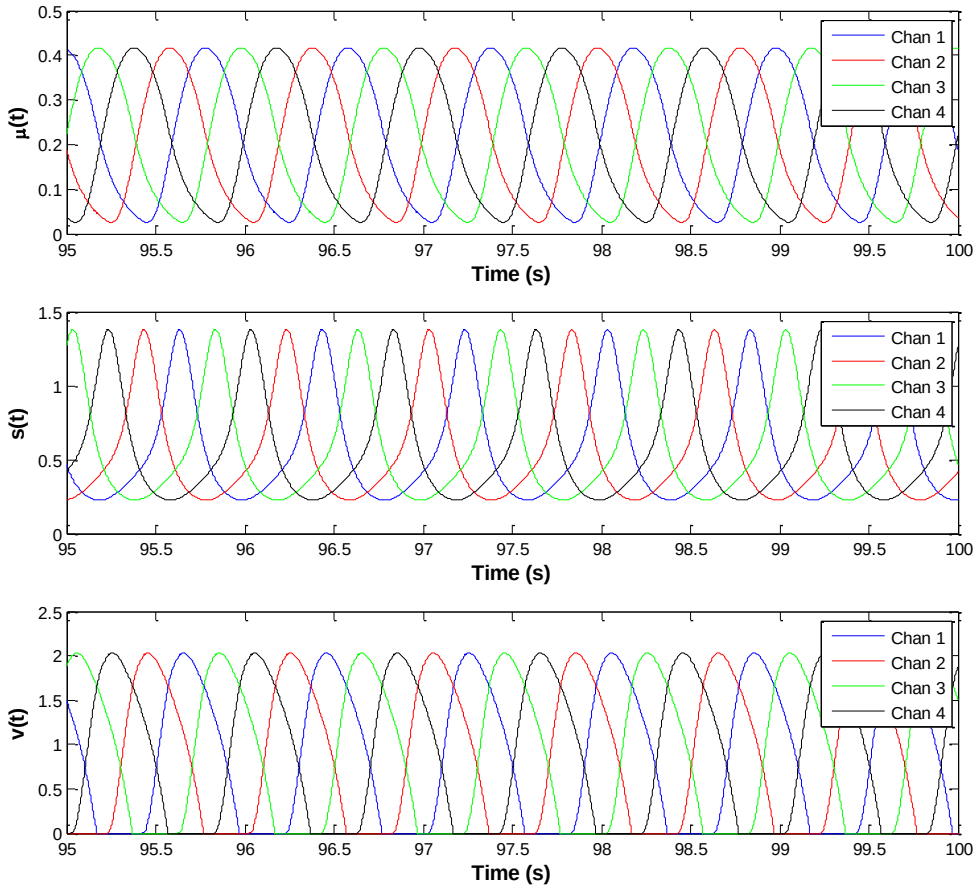

Figure 10. Fully converged limit cycle results for Case C-4G (TH variables).

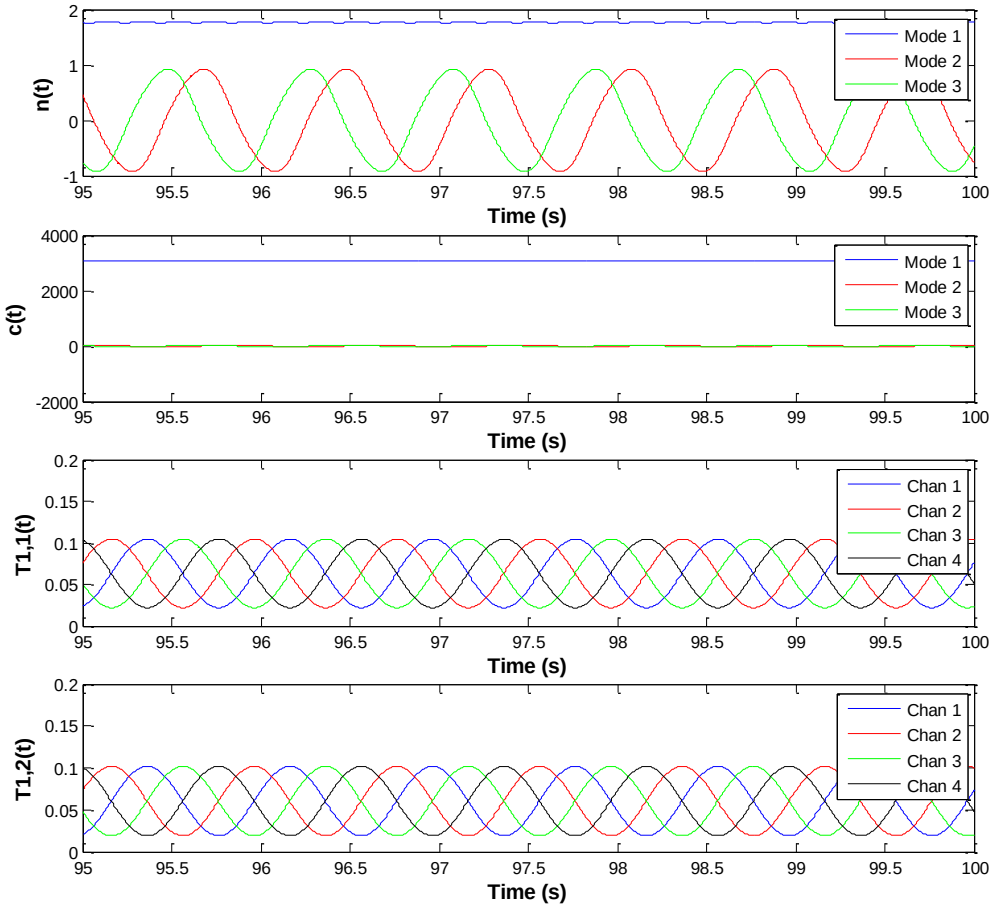

Figure 11. Fully converged limit cycle results for Case C-4G (neutronic variables).